Ground-based transmitter signals observed from space: ducted or nonducted?

Mark A. Clilverd[1], Craig J. Rodger[2], Rory Gamble[2], Nigel P. Meredith[1], Michel Parrot[3], Jean-Jacques Berthelier[4] and Neil. R. Thomson[2]

Prepared for Journal of Geophysical Research – Space Physics

21 June, 2007

[1] M. A. Clilverd and N. P. Meredith, Physical Sciences Division, British Antarctic Survey, High Cross, Madingley Road, Cambridge CB3 0ET, England, U.K. (email: macl@bas.ac.uk ; nmer@bas.ac.uk)

[2] R. Gamble, C. J. Rodger and N. R. Thomson, Physics Dept., University of Otago, Dunedin, New Zealand. (email: rgamble@physics.otago.ac.nz ; crodger@physics.otago.ac.nz, n_thomson@physics.otago.ac.nz)

[3] M. Parrot, Laboratoire de Physique et Chimie de l'Environnement, 3A Avenue de la Recherche Scientifique, 45071 Orleans Cedex 2, France (email: mparrot@cnrs-orleans.fr).

[4] J-J Berthelier, Centre d'Etudes des Environnements Terrestre et Planétaires, 4 Avenue de Neptune, Saint Maur des Fosses, France. (email: jean-jacques.berthelier@cetp.ipsl.fr)

(Received N x, 2007; N x 27, 2007;

accepted N x, 2007.)

Abstract. The principal loss mechanism for electrons from the inner radiation belt (1.2<L<2.0) and slot region (2.0<L<3.0) is atmospheric precipitation driven by several processes, including coulomb collisions, plasmaspheric hiss, lightning-generated whistlers, and man-made transmissions. Several studies have shown that ducted and nonducted VLF waves can precipitate radiation belt energetic electrons into the upper atmosphere. Here we investigate the propagation of VLF communication transmitter signals using plasma wave instruments onboard the CRRES and DEMETER satellites in order to determine if nonducted transmitter signals are significant in radiation belt loss processes. We investigate the regions where strong transmitter signals are observed in the ionosphere directly above the transmitter, in the magnetosphere near where the signals cross the geomagnetic equator, and in the ionospheric region geomagnetically conjugate to the transmitter. For very low L-shell transmitters (L<1.5) there is evidence that a significant proportion of the wave energy propagating into the plasmasphere is nonducted. However, at higher L-shells the waves become highly ducted in the plasmasphere. Strong evidence for this comes from the lack of significant wave power propagating above the electron half gyro-frequency limit for inter-hemispherically ducted waves. We conclude that man-made transmissions in the frequency range (18-25 kHz) will be restricted to driving electron precipitation primarily from the inner radiation belt (L=1.3-2.5). This will come about through a combination of propagation types, partly through nonducted wave propagation at very low L-shells (L=1.3-1.5), but predominantly through ducted wave propagation at higher L-shells (L=1.5-2.5), ultimately limited by the electron half-gyro frequency limit for ducted waves.

1. Introduction

High energy electrons trapped in the Earth's Van Allen radiation belts are distributed into two belts divided by a relatively low flux region known as the 'electron slot region' at L~2.5 [Van Allen et al., 1958; Van Allen, 1997]. The principal source and loss mechanisms that control the radiation belt electrons are still under investigation, although the losses are known to be due to a combination of several mechanisms, including coulomb collisions, and resonant wave-particle interactions with plasmaspheric hiss, lightning-generated whistlers, and man-made transmissions [e.g., Abel and Thorne, 1998a, 1999, Rodger et al., 2003, Meredith et al., 2006; 2007]. Recently, Rodger et al. [2006] considered the impact of a sudden injection of high energy particles into the radiation belts either through a high altitude nuclear explosion or a natural injection from intense solar activity. Potential damage to orbiting satellites could be mitigated by enhanced removal of the energetic electrons through accelerated loss rates possibly driven by ground-based VLF communication transmitters. The topic is generally known as Radiation Belt Remediation (RBR) which provide some level of human control of the trapped electron populations in the radiation belts.

Ground based VLF transmitters operate near-continuously with radiated powers as large as 1 MW. A portion of the transmitter signals propagate through the ionosphere into the magnetosphere, where they are able to precipitate radiation belt electrons into the upper atmosphere through cyclotron resonance interactions. The majority of transmitters operate in the frequency range 18-25 kHz and are located on geomagnetic field lines in the range 1.1<L<4.0. Previous theoretical studies into the impact of VLF transmitters on the radiation belt electron population [e.g., Abel and Thorne, 1998a] have generally relied on techniques based on magnetospherically ducted propagation alone [e.g. Inan et al., 1984]. Ducted waves experience equatorial gyro-resonant interactions with electrons typically in a narrow energy range of only a few tens of keV, depending on transmitter frequency, location, and the wave propagation conditions described by magnetic field intensity, plasma number density, and wave propagation angle [Datlowe and Imhof, 1990]. For example, for a ducted 20 kHz transmitter wave at L=2.0 the equatorial resonant electron energy would be 50 keV. As a result VLF transmitters were not considered to be significant for the radiation belt loss rates, or as a source of precipitating energetic electrons into the upper atmosphere. However, several studies have shown that a combination of ducted and nonducted VLF waves from lightning-generated whistlers and communication transmitters can efficiently precipitate radiation belt energetic electrons into the upper atmosphere through equatorial gyro-resonance [Kennel and Petschek, 1966], Landau and higher resonances [Abel and Thorne, 1998b], and off-equatorial gyro-resonance [Johnson et al., 2001; Lauben et al., 1999; Peter and Inan, 2004; Inan et al., 2007]. Datlowe and Imhof [1990] suggested that SEEP data showing extended L-shell ranges of equatorial cyclotron resonant electron precipitation from VLF transmitters had energies consistent with ducted wave normal angles, but they argued for nonducted wave propagation because of the lack of discrete striations in L-shell as would be expected by ducted interactions. Nonducted VLF waves propagate such that they could rapidly spread throughout large portions of the inner magnetosphere, resonantly interacting with a broad range of high energy electrons, with highest energies typically >100 keV

[Bortnik et al., 2006a]. As a result VLF transmitter signals could be considered as a significant loss mechanism for the radiation belts and thus potentially useful for RBR.

Resonant pitch angle scattering of electrons by nonducted whistler waves has been described by Jasna et al. [1992] and developed into a quantitative model by Lauben et al. [1999]. Further development of the model has been undertaken by Bortnik et al. [2006a]. In contrast to the traditional picture of ducted propagation, the nonducted waves more readily spread throughout the plasmasphere, particularly polewards of the radiating lightning discharge or transmitter source location [Bortnik et al., 2006a]. Calculations using whistler signals spanning the frequency range 0.2-60 kHz show that for sources at $L \leq 2.0$ the waves propagate to higher L-shells in the plasmasphere as a result of being nonducted, and produce electron precipitation at ~10º higher latitudes than the source location. For sources at $L \sim 3.0$ calculations show that there is less poleward propagation of the whistler waves and the electron precipitation tends to begin at the source latitude, extending less distance polewards than for the lower latitude sources [Bortnik et al., 2006b]. Confirmation of the nonducted whistler wave model has been suggested by Inan et al. [2007] using the Hawaii VLF transmitter NPM at L=1.17 to precipitate electrons at L=2.0, and at higher energies than predicted by ducted gyro-resonant interactions (> 100 keV).

Ground-based receivers of inter-hemispheric whistler-mode signals have been used to monitor several VLF transmitters that are relevant to this topic. Andrews [1978] and Thomson [1987a, 1987b] discussed two groups of whistler signals observed in the conjugate region of the Hawaii VLF transmitter. One group was inter-hemispherically ducted whistler-mode signals propagating over a range of 1.5<L<2.5, and the other was nonducted very low latitude signals propagating close to L~1.1. Saxton and Smith [1989] analysed inter-hemispherically ducted whistler-mode signals from the NAA and NSS transmitters located in the eastern U.S.A, and observed signals over a range of $2.2<L<2.7$, while using the same transmitters Clilverd et al. [2000] observed signals at $1.8<L<2.8$, and Clilverd and Horne [1996] observed signals at $1.7 < L < 2.6$. All of these ground-based measurements showed an upper L-shell of propagation close to the electron half gyrofrequency cut off limit for inter-hemispherically ducted propagation as would be expected for a field-aligned wave normal that was able to penetrate the ionosphere [Strangeways, 1981]. The lower L-shell limit is consistent with the inability of the propagating waves to be guided by very non-vertical field lines at such low geomagnetic latitudes.

Some calculations using wave propagation models have suggested that waves can be subject to severe cyclotron resonant absorption at ~1/3 of the electron gyrofrequency and would therefore not be observable at ionospheric altitudes in the conjugate hemisphere [Thorne and Horne, 1996], and that this effect might be more influential than the electron half gyrofrequency cut off limit. Smith et al. [2001] used whistler signals from L=3.0-4.5 to determine that the output power of field-aligned whistlers did reduce with increasing L-shell in broad agreement with Thorne and Horne [1996]. Clilverd and Horne [1996] also showed that for conjugate NAA signals there was enhanced absorption of the signals for $L>2.0$. However, in their studies of the NAA and NSS transmitter signal propagation, Clilverd et al. [2000] in geomagnetically active times, and Saxton and Smith [1989] in geomagnetically quiet times, showed that ~70%-95% of the observed conjugate signals propagated at L-shells above the 1/3 electron gyrofrequency (L~2.3), while only 1%-6% propagated just above the 1/2 electron gyrofrequency cut off limit (L~2.6), and none at L>2.7. This strongly suggests that the 1/2 electron gyrofrequency cut off limit is the main influence on the ducted signals studied in this paper.

Thus we would expect ducted signals to be constrained to propagate inter-hemispherically between the L-shells of 1.5<L<2.5 for the frequencies used by powerful VLF transmitters. While nonducted signals should either propagate polewards of the transmitter locations, and not be constrained by the electron half gyro-frequency cut off limit for inter-hemispherically ducted signals [Johnson et al., 2001; Peter and Inan, 2004; Inan et al., 2007], or be constrained by strong cyclotron damping above 1/3 the electron gyro-frequency [Thorne and Horne, 1996]. These differences can be used as a test to determine the relative proportions of these two wave propagation mechanisms.

In this study we investigate the nighttime propagation of VLF communication transmitter signals using plasma wave instruments onboard the CRRES and DEMETER satellites. We investigate the regions where strong transmitter signals are observed in the ionosphere directly above the transmitter, in the magnetosphere close to the geomagnetic equator, and in the ionospheric region geomagnetically conjugate to the transmitter. Using these observations we discuss the propagation characteristics in terms of the proportions of ducted or nonducted signals, and thus characterize the likely impact of nonducted VLF transmitter signals on the radiation belt populations.

2. Wave data from DEMETER and CRRES satellites

DEMETER is the first of the Myriade series of microsatellites developed by the Centre National d'Etudes Spatiales for low-cost science missions, and was placed in a circular Sun-synchronous polar orbit at an altitude of 710 km at the end of June 2004. Data are available at invariant latitudes <65º, providing observations around two local times (~10:30 LT and 22:30 LT). The Instrument Champ Electrique (ICE) on the DEMETER spacecraft provides continuous measurements of the power spectrum of one electric field component in the VLF band [Berthelier et al., 2006]. The ICE experiment consists of 4 electric field sensors mounted on each end of 4 stacer booms, such that any pair of sensors can be used to determine the electric field along the axis defined by the two sensors. As a result the three components of DC and AC vector electric field can be obtained. The signals are sampled at 40 kHz, averaged to a temporal resolution of 2.048 s and telemetered to the ground. In this study we make use of both survey and burst mode power spectrum data recorded up to 20 kHz, with a frequency channel resolution of 19.25 Hz. We particularly concentrate on narrow-band transmissions close to 20 kHz, which are produced by powerful man-made radio communication systems at known locations around the world. The DEMETER orbit is such that we are able to map out the received signal strength of each narrow frequency band in the ionosphere above the transmitter location, and in the conjugate region in the opposite hemisphere. In this study we make use of the data observed in the nighttime orbits (22:30 LT) because of the significant reductions in ionospheric absorption of the transmitter signals during the nighttime in comparison with the day [Clilverd et al., 1993]. We use wave data from successive orbits, averaged over a study period lasting several weeks, in order to improve the signal to noise ratio. In this study we describe DEMETER observations projected to 100 km altitudes using the IGRF (2000) magnetic field model, plotted with a resolution of 2º × 2º.

Unlike DEMETER, which is in low Earth orbit, the Combined Release and Radiation Effects Satellite (CRRES) was launched on 25 July 1990, and operated in a highly elliptical geosynchronous transfer orbit with a perigee of 305 km, an apogee of 35,768 km and an inclination of 18°. The orbital period was approximately 10 hours, and the initial apogee was at a magnetic local time (MLT) of 0800 MLT. The magnetic local time of apogee decreased at a rate of approximately 1.3 hours per month until the satellite failed on 11 October 1991, when its apogee was at about 1400 MLT. The satellite swept through the plasmasphere on average approximately 5 times per day for almost 15 months. The Plasma Wave Experiment provided measurements of electric fields from 5.6 Hz to 400 kHz, using a 100 m tip-to-tip long wire antenna, with a dynamic range covering a factor of at least 10^5 in amplitude [Anderson et al., 1992].

The sweep frequency receiver, which is used in this study, covered the frequency range from 100 Hz to 400 kHz in four bands with 32 logarithmically spaced steps per band, the fractional step separation being about 6.7% across the entire frequency range. We are particularly interested here in Band 3 (6.4 to 51.7 kHz), which was sampled 4 times per second with complete cycling times of 8.192 s. In this experiment the bandwidth of each narrow-band frequency channel was typically 900 Hz, which is wide in comparison with the man-made transmissions, which typically have ~200 Hz effective bandwidth. Additionally the center frequency of each channel had not been selected with the transmitter frequencies in mind. However, we have selected those channels that contain, and are dominated by, signals from known transmitters, e.g. the 23.8 ± 0.45 kHz channel which contains the 24.0 kHz transmitter located in Cutler, Maine, USA (known by its call sign of "NAA").

As a result of the highly elliptical geosynchronous transfer orbit, we use CRRES observations that are made within ±30º of the geomagnetic equator near the magnetic field lines whose foot prints in the ionosphere end close to the known location of transmitters. In this study we describe CRRES observations projected to 100 km altitudes, plotted with a resolution of 5º × 5º. The position of the CRRES spacecraft is mapped to the ionosphere using the IGRF 85 model corrected for external magnetospheric currents by the Olson-Pfitzer tilt dependent static model [Olson and Pfitzer, 1977]. This is the standard process used to analyze all CRRES data. In this way we complement the DEMETER observations, such that we follow the wave power from each of the transmitters studied, first in the ionosphere above it, then on the field line near the geomagnetic equator, and then finally in the ionosphere in the conjugate region. Thus we investigate the comparative influences of ducted and nonducted wave propagation through the plasmasphere.

3. Results

(i) VLF transmitters located in the range 1.3<L<2.0

In Figure 1 we combine the observations from DEMETER and CRRES from the narrow-band transmitter (call sign NWC) located at the NorthWest Cape of Australia (21.8ºS, 114.1ºE, L=1.44 at 100 km altitude). This transmitter operated at 19.8 kHz in 2005 and 22.3 kHz in 1990/91. The plot shows the average nighttime wave spectral power from CRRES ($mV^2m^{-2}Hz^{-1}$) on the right hand panel and the difference between average wave intensity and the local background from DEMETER ($\mu V^2 m^{-2} Hz^{-1}$) on the left. The numbers on the two colour bars differ by about 9 orders of magnitude, 6 are due to the difference in units (mV^2 and μV^2), and the rest is consistent with changes in signal strength due to the altitude difference of the two satellite measurements. A cross shows the location of the transmitter in the southern hemisphere, and a diamond shows the equivalent conjugate point in the northern hemisphere. The DEMETER observations are averaged during nighttime conditions from 12 August to 26 September 2005, and cover the frequency band 19.795 ± 0.01 kHz. In order to remove lightning noise appearing at the same frequency as NWC we have subtracted the average power detected in the frequency channels 195 Hz (i.e., 10 frequency channels) above and below the transmitter frequency from the 19.795 ± 0.01 kHz transmitter band. This type of plot will be termed the 'difference' plot. Using 'difference' plots is not necessary for CRRES data because the lightning noise is less significant than for DEMETER, most likely because of the long period averaging undertaken for CRRES data. The CRRES observations cover the whole of the satellite lifetime from July 1990 to October 1991, with data selected for nighttime conditions (18-06 MLT) and the channel 22.5 ± 0.45 kHz. This frequency range covers the NWC frequency at that time, of 22.3 kHz. Because we do not do difference plots for the CRRES data the figures show the "true" power across its frequency channel.

In the southern hemisphere the wave power peaks above the transmitter location and is essentially symmetrical about it. There appears to be some evidence of banded structure at large distances from the transmitter. This is consistent with the structure expected from modal interference in the subionospheric waveguide. Similar structures have been previously reported in DEMETER wave data near the NWC transmitter [Molchanov et al., 2006]. In the northern hemisphere the wave power peaks in a region polewards of the conjugate point, but is still essentially symmetrically positioned in longitude relative to the transmitter conjugate point. The CRRES observations presented here were made at the geomagnetic equator on field lines from L=1.2 to L=6 during 1990-1991. To show them more clearly the observations have been projected to ionospheric altitudes on the field line that the observations were made. The data projected to the northern hemisphere is the same as that shown in the southern hemisphere, any differences are due to the divergence of the magnetic field lines from hemisphere to hemisphere. The regions of channel wave power observed by CRRES closely overlap the regions mapped out by DEMETER. However, CRRES observations at the lowest latitudes are restricted by the 0.1 L binning of the CRRES data, because as a result of the binning the magnetic field footprint becomes more spread than the $5^{o} \times 5^{o}$ geographical resolution that we use in this study, and therefore the data are not used.

To show the inter-comparison between DEMETER and CRRES more clearly we identify the regions of peak spectral power associated with the NWC transmitter as regions where the wave intensity above the local background is $>3\times10^{2}$ $\mu V^{2}m^{-2}Hz^{-1}$ in the DEMETER 'difference' plot, and $>10^{1}$ $\mu V^{2}m^{-2}Hz^{-1}$ for CRRES data ($>10^{-5}$ $mV^{2}m^{-2}Hz^{-1}$ on the colour scale in Figure 1), and plot them in Figure 2 on a map of the region. The areas shown in the plot are similar despite different thresholds for the two satellites as a result of the altitude that the measurements were made. The cross in Figure 2 represents the location of the NWC transmitter and the diamond identifies its conjugate point. The solid line shows the DEMETER peak spectral energy regions in the transmitter's hemisphere, and the DEMETER peak spectral energy in the conjugate region, while squares show the CRRES equatorial peak intensity region projected from the geomagnetic equatorial region into the conjugate hemisphere. The L-shell contour of the electron half gyro-resonant frequency propagation limit for ducted waves with a frequency of 19.8 kHz is also marked on the plot. This represents the L-shell of the field line below which ducted waves are able to propagate into the conjugate hemisphere and remain field-aligned. Also shown is the contour line of the L=1.5, 2.0, and 2.5 L-shells. L=1.5 marks the approximate lower limit of observed inter-hemispherically ducted wave propagation in the plasmasphere [Thomson, 1987b].

Using Figure 2 we can see that most of the conjugate wave power from NWC has propagated poleward of the transmitter, and is principally contained between the L=1.5 contour and the half gyro-frequency cut off limit for inter-hemispherically ducted signals (the L=2.80 contour for 19.8 kHz waves). The CRRES equatorial peak intensity region projected into the conjugate hemisphere closely overlaps the DEMETER conjugate peak wave power region, and both are centered about 10° of latitude north of the conjugate point. In comparing the CRRES and DEMETER regions we see that the CRRES-observed transmissions propagate further westward than DEMETER. This may be due to different horizontal electron density gradients occurring during the two different satellite data collection periods, i.e., CRRES during solar maximum and DEMETER during solar minimum. Ionospheric electron density gradients have previously been shown to significantly influence the propagation longitudes of the same VLF transmitters that are being studied here [Clilverd et al., 1992a,b].

A second example of the propagation of signals from a transmitter located in the 1.3 <L< 2.0 range is given in Figure 3. The transmitter is HWU (L=1.83) operating at 18.3 kHz in France. DEMETER difference observations centered on the frequency range 18.29 ± 0.01 kHz are plotted with CRRES observations in the frequency range 18.5 ± 0.45 kHz. The plot is the same format as Figure 1. The regions of peak wave power were identified and plotted in Figure 4 using the same format as Figure 2. Once again, the majority of the wave power is contained between the L=1.5 contour and the electron half gyro-frequency cut off limit for inter-hemispherically ducted signals (the L=2.88 contour for 18.3 kHz waves), and some outside of the1/3 electron gyro-frequency cut off limit (L=2.5 for 18.3 kHz waves). The CRRES equatorial peak intensity region projected into the conjugate hemisphere closely overlaps the DEMETER conjugate peak wave power region. Both satellites suggest that the peak wave power is centered about 5º-10 º poleward of the transmitter conjugate point. As in Figure 2 there is a displacement between the two highlighted regions, eastward this time, also possibly due to differences in horizontal ionospheric gradients occurring during the CRRES and DEMETER lifetimes. However, this should be tested by 3D ray-tracing.

(ii) VLF transmitters located in the range 2.0<L<3.0

An example of the signals from a transmitter located at higher latitudes is shown in Figure 5, where the plot follows the formats of Figures 1 and 3. The transmitter is NAA (L=2.93) operating at 24.0 kHz in Maine, USA. The CRRES observations are taken from the frequency range 23.8 ± 0.45 kHz, but the DEMETER observations are taken from

16.0 kHz because the strong NAA signals are aliased from 4 kHz above the 20 kHz Nyquist frequency of the wave instrument to 4 kHz below it. This effect in DEMETER wave observations is also observed for the signals from 23.4 kHz (call sign DHO in Germany) aliased to 16.6 kHz, and 21.4 kHz (NPM in Hawaii) aliased to 18.6 kHz. In this case the DEMETER data shown are taken from 01 January 2005– 02 February 2005, and are differenced with data from ± 195 Hz either side of the central frequency in the same way as in Figures 1 and 3. We use January 2005 data in this case because the aliased NAA signal is weak and January has less background lightning noise in the North American region than in August. The DEMETER data clearly shows a modal minimum feature ~20º in latitude from the transmitter. This corresponds to ~2200 km, which is consistent with the location of a D-region modal minimum in the NAA nighttime interference pattern identified by Clilverd et al. [1999], based on the times of sunrise modal minima on the NAA transmitter signal, observed from Antarctica.

The regions of peak wave power were identified and plotted in Figure 6 using the same format as Figure 2 and 4. The peak wave power above the local background in the DEMETER data is defined by a region inside the contour of 1 $\mu V^2 m^{-2} Hz^{-1}$. This is much lower than the threshold used in Figures 2 and 4, but is weaker because of the aliasing of the transmitter frequency into the DEMETER frequency range. However, for this plot we have also added the electron gyro-frequency L-shell contour as we would not expect any waves, ducted or nonducted, to be able to propagate outside of this limit. Once again, the majority of the wave power is contained between the L=1.5 contour and the electron half gyro-frequency cut off limit for inter-hemispherically ducted signals (the L=2.63 contour for 24.0 kHz waves), and significant proportions propagate outside of the1/3 electron gyro-frequency cut off limit (L=2.3 for 24.0 kHz waves). The CRRES equatorial peak intensity region projected into the conjugate hemisphere closely overlaps the DEMETER conjugate peak wave power region. Both satellites suggest that the peak wave power is centered about 9º equatorward of the transmitter conjugate point, 6º equatorward of the electron half gyro-frequency limit, whereas the NAA conjugate is 3º polewards of the electron half gyro-frequency limit.

Non-difference DEMETER measurements of the power above the NAA transmitter (x in Figure 5, left-hand panel) and at NAA's conjugate point (◊ in Figure 5 left-hand panel) show that the power at the conjugate point is smaller by a factor of 170 than above the transmitter. Although the powers shown in the figure are not absolute because of the aliasing of the 24.0 kHz signal into the 16.0 kHz frequency band, the ratio of the conjugate powers is enlightening as it is much larger than we found for the NWC transmitter (a factor of 4 reduction from transmitter to conjugate ionosphere). In the case of NAA the peak power in the conjugate hemisphere is located equatorwards of the L-shell of the electron half gyro-frequency, where it is ~17 times stronger than at NAA's conjugate point. This result clearly identifies that the majority of the signals from NAA, observed by DEMETER in the conjugate region, are being restricted by the electron half gyro-frequency and are therefore ducted.

In Figure 7 we plot the equatorial region of peak wave power from the CRRES observations for the 21.4 kHz transmitter (call sign NSS, L=2.43) located near Washington, USA. We do not show the DEMETER observations because none are available for this transmitter, as NSS was permanently de-commissioned prior to the launch of the satellite. Once again most of the wave power is contained between the L=1.5 contour and the half gyro-frequency cut off limit for inter-hemispherically ducted signals (the L=2.73 contour for 21.4 kHz waves), and significant proportions propagate outside of the1/3 electron gyro-frequency cut off limit (L=2.39 for 21.4 kHz waves). Most of the wave power is centered about 4º equatorward of the transmitter conjugate point.

(iii) VLF transmitters located in the range 1.0<L<1.3

Finally, in Figure 8 we show the regions of peak wave power from the Hawaii transmitter (NPM, 21.4 kHz, L=1.17). The format of the plot is the same as Figures 2, 4, 6, and 7. This transmitter is located at a very low L-shell. No CRRES observations of the signals from this transmitter are available. At the time of the CRRES mission the transmitter was operating at 23.4 kHz and that frequency is just on the edge of the CRRES channel used to observe NAA in Figure 5. But no region of peak wave power close to the location of NPM is detectable in the CRRES data. Figure 8 therefore shows the regions of peak wave power derived from DEMETER observations made at the aliased transmitter frequency of 18.6 kHz. The conjugate signals from the transmitter are typically located between 1.2 <L< 1.5, at lower latitudes than the range expected for inter-hemispherically ducted whistler-mode signals and at such low latitudes that the half gyro-frequency limit on ducted propagation is not significant. The poleward displacement of the region of peak wave power is 7º. There is also a westwards displacement (~10º) of the peak power, which as discussed earlier, is possibly due to the influence of horizontal electron density gradients in the ionosphere [Clilverd et al., 1992a,b].

4. Discussion

The lowest L-values that significant inter-hemispheric wave power from NAA, NSS, and HWU is observed by our satellites are in the range L=1.5-1.7. This result is consistent with the lower limits of ducted wave propagation previously observed by ground-based experiments [Andrews, 1978; Clilverd and Horne, 1996] using the same transmitters. This suggests a strong influence of ducting on the propagation of transmitter signals in the plasmasphere. In contrast, the very low latitude transmitter NPM (L=1.17) produces peak wave power in the conjugate hemisphere in the range $1.2<L<1.5$. This is completely at odds with the L-shell range of ducted signals ($1.5<L<2.5$) received by long-running ground-based experiments observing the same transmitter [Thomson, 1987b]. This DEMETER observation, made at 710 km altitude in the conjugate region to the transmitter, suggests that most of the plasmaspheric propagation from NPM is nonducted. The observations also show that nonducted signals are detectable by DEMETER, and that our conclusions showing little nonducted wave power from NAA, NSS and HWU based on DEMETER data are reasonable.

When calculating electron precipitation fluxes and energy spectra from transmitters in the 18-25 kHz frequency range, there are different outcomes depending on the proportions of ducted and nonducted waves and if the wave-particle interaction region is confined to the geomagnetic equator or is off-equatorial. Nonducted wave models predict regions of peak conjugate wave power and electron precipitation at L-shells that are displaced polewards of the latitude of the source transmissions, particularly for sources at L<3.0, and that the energy spectra would be harder than expected for ducted waves [Bortnik et al, 2006a; Inan et al., 2007]. Because of the nonducted nature of the waves, the conjugate peak wave power would not be expected to coincide with the precipitation region [Lauben et al., 2001], because the wave is still propagating outward in L-shell after passing the geomagnetic equatorial region. Ducted wave models would predict electron precipitation occurring typically over the range 1.5 <L< 2.8 for these transmitter frequencies, independent of the L-shell of the source transmissions, and that the geographical location of the precipitation would be associated with the region of peak wave power.

Datlowe and Imhof [1990] used SEEP satellite observations made at ~250 km in 1982, and observed electron precipitation from the NWC, NSS, and NAA transmitters. The precipitated electron energy spectra caused by NWC ranged from 40-200 keV in the L-shell range L=1.6-2.0. L=2.0 was the upper limit of the study. No precipitation was observed below L=1.6. In 1982 the L-shell of NWC was L=1.42. Thus the electron precipitation occurred polewards of the transmitter, consistent with the region of peak wave power found in this study, and with energies consistent with parallel propagation of ducted waves [Datlowe and Imhof, 1990]. Electron precipitation from NAA and NSS was also observed in the L-shell ranges 1.6-2.0, and with energies consistent with parallel propagation of ducted waves, particularly when taking into account the influence of the high background electron density values occurring at American longitudes near the December solstice [Clilverd et al., 1991, 2007]. Both the confinement in L-shell of the precipitation and the precipitated electron energy spectra driven by all of these transmitters suggest that the wave power from VLF transmitters is primarily ducted in the plasmasphere. The Datlowe and Imhof results are also consistent with our suggestion that the NWC waves between L=1.4-1.6 are nonducted, and that the waves do not cause any significant electron precipitation at these locations.

For sources at higher latitudes the results from NSS (L=2.43), and NAA (L=2.93) show significant influence of the electron half gyro-resonance limit for ducted propagation, and are consistent with ducted propagation being dominant. In the middle range of latitudes, where transmission sources are NWC (L=1.44) and HWU (L=1.83), the L-shell range of wave power observed in the conjugate region is generally consistent with the range expected for ducted propagation. However, NWC (L=1.44) does produce some conjugate wave power at lower L-shells (L~1.4), and this is indicative of some nonducted power at these L-shells. Any electron precipitation from the nonducted waves would be expected to occur polewards of L=1.4 and as a result would occur close to the L-shell of peak wave power observed by both DEMETER and CRRES (L~1.6-2.0) the expected location for electron precipitation caused by ducted waves.

The results presented here from NPM (L=1.17) are consistent with the dominance of nonducted signals propagating from this source into the plasmasphere. The displacement of the conjugate wave power peak at L~1.4 from the region seen occasionally by ground-based observations of ducted waves (L>1.5), and the L~2.0 electron precipitation region from NPM described by Inan et al. [2007] strongly suggest nonducted propagation. Datlowe and

Imhof [1990] found that no electron precipitation could be observed from NPM for L<2.0, which is consistent with low efficiency of electron scattering by nonducted lightning-generated waves [Meredith et al., 2007].

In Table 1 we summarize the likely electron precipitation energies expected from each transmitter described in this study based on the L-shells of the peak wave power observed in this study, the transmitter frequency, and assuming parallel (0 deg wave normal angle) cyclotron resonance interactions at the geomagnetic equator on each of the field lines [Datlowe and Imhof, 1990]. We are unable to estimate the energy range for nonducted NPM waves; however, we note here that the ducted electron precipitation energy would be ~0.5 MeV. NWC is shown to be the most effective transmitter in terms of the largest energy range of precipitation energies, and is also well positioned in being west of the South Atlantic Anomaly which provides increased sensitivity of the loss of scattered electrons into the drift loss cone [Datlowe and Imhof, 1990].

5. Summary

In this study we have observed the wave propagation characteristics of signals from transmitters located in the range 1.1<L<3.0. Contrary to the idea of significant proportions of nonducted waves propagating in the plasmasphere, and this propagation path being dominant in comparison to ducted waves, we detect little wave power propagating at the L-shells above the electron half gyro-frequency limit for inter-hemispherically ducted waves.

This is a test for ducted wave propagation and is confirmed by both CRRES close to the geomagnetic equator and DEMETER in the conjugate region of the transmitters.

For very low L-shell transmitters (L<1.5) there is evidence that significant proportions of the wave energy propagating into the plasmasphere is nonducted. At higher L-shells (L>1.5) the evidence is that the waves become highly ducted in the plasmasphere. This picture is consistent with the ray-tracing results of Strangeways [1981] whose work showed that the orientation of the magnetic field lines to the near-vertically propagating waves as they pass through the ionosphere limits the effectiveness of the trapping of waves into ducts. Signals from very low L-shell transmitters are unable to trap into ducts and are therefore nonducted. Signals from transmitters at higher L-shells are more easily trapped and become increasingly ducted. As a result the expected electron precipitation from these transmissions is likely to be confined in L-shell and result in a softer energy spectrum than the nonducted transmissions. Man-made transmissions in the frequency range studied here (18-25 kHz) will thus be restricted to driving electron precipitation primarily from the inner radiation belt (L=1.3-2.5). This will come about through a combination of propagation types, partly through nonducted wave propagation at very low L-shells (L=1.3-1.5), but predominantly through ducted wave propagation at higher L-shells (L=1.5-2.5). This L-shell range is broadly consistent with the spatial region where the results of Abel and Thorne [1998a] predict that scattering from VLF transmitters should dominate energetic electron lifetimes.

We show that NWC in Australia is particularly well placed to influence the radiation belt electron population in the inner radiation belt, with electron precipitation likely to occur in the 30-750 keV range. This energy range is a function of NWC's current transmission frequency, and the latitudinal spread of the ducted waves from the transmitter.

Acknowledgments. The authors would like to thank Luke S. Stewart and Robert McCormick, of the University of Otago, for initial software development.

References

Abel, B., and R. M. Thorne (1998a), Electron scattering loss in earth's innermagnetosphere-1. Dominant physical processes, J. Geophys. Res., 103, 2385–2396.

Abel, B., and R. M. Thorne (1998b), Electron scattering loss in Earth's inner magnetosphere 2. Sensitivity to model parameters, J. Geophys. Res., 103(A2), 2397-2408, 10.1029/97JA02920.

Abel, B., and R. M. Thorne (1999), Correction to "Electron scattering loss in earth's inner magnetosphere, 1. Dominant physical processes" and " Electron scattering loss in earth's inner magnetosphere, 2. Sensitivity to model parameters" by Abel, B. and Thorne, R. M., J. Geophys. Res., 104, 4627–4628.

Anderson, R. R., D. A. Gurnett, D. I. Odem (1992), CRRES Plasma-Wave Experiment, J. Spacecraft Rockets, 29 (4), 570-573.

Andrews, M. K. (1978), Non-ducted whistler-mode signals at low latitudes, J. Atmos. Terr. Phys., 40, 429-436.

Berthelier, J.J. et al. (2006), ICE, The electric field experiment on DEMETER, Planet. Space Sci., 54 (5), Pages 456-471.

Bortnik, J., U. S. Inan, and T. F. Bell (2006a), Temporal signatures of radiation belt electron precipitation induced by lightning-generated MR whistler waves: 1. Methodology, J. Geophys. Res., 111, A02204, doi:10.1029/2005JA011182.

Bortnik, J., U. S. Inan, and T. F. Bell (2006b), Temporal signatures of radiation belt electron precipitation induced by lightning-generated MR whistler waves: 2. Global signatures, J. Geophys. Res., 111, A02205, doi:10.1029/2005JA011398.

Clilverd, M. A., A. J. Smith, and N. R. Thomson (1991), The annual variation in quiet time plasmaspheric electron density determined from whistler mode group delays, Planet. Space Sci., 39, 1059-1067.

Clilverd, M. A., A. J. Smith, and N. R. Thomson (1992a), The effects of horizontal ionospheric electron-density gradients on whistler mode signals, J. Atmos. Terr. Phys., 54, 1061-1074.

Clilverd, M. A., N. R. Thomson, and A. J. Smith (1992b), Observation of 2 preferred propagation paths for whistler-mode VLF signals received at a nonconjugate location, J. Atmos. Terr. Phys., 54, 1075-1079.

Clilverd, M. A., N. R. Thomson, and A. J. Smith (1993), The influence of ionospheric absorption on midlatitude whistler-mode signal occurrence from VLF transmitters, J. Atmos. Terr. Phys., 55, 1469-1477.

Clilverd, M. A., and R. B. Horne (1996), Ground-based evidence of latitude-dependent cyclotron absorption of whistler mode signals originating from VLF transmitters, J. Geophys. Res. Vol. 101, p. 2355-2368 (95JA03153).

Clilverd, M. A., N. R. Thomson, and C. J. Rodger (1999), Sunrise effects on VLF signals propagating over a long north-south path, Radio Sci., 34, 939-948.

Clilverd, M. A., B. Jenkins, and N. R. Thomson (2000), Plasmaspheric storm time erosion, J. Geophys. Res., 105, 12,997–13,008.

Clilverd, M. A., N. P. Meredith, R. B. Horne, S. A. Glauert, R. R. Anderson, N. R. Thomson, F. W. Menk, and B. R. Sandel (2007), Longitudinal and seasonal variations in plasmaspheric electron density: Implications for electron precipitation, J. Geophys. Res., 112, A11210, doi:10.1029/2007JA012416.

Datlowe, D. W., and W. L. Imhof (1990), Cyclotron resonance precipitation of energetic electrons from the inner magnetosphere, J. Geophys. Res., 95, 6477-6491.

Inan, U. S., H. C. Chang, and R. A. Helliwell (1984), Electron precipitation zones around major ground-based VLF signal sources, J. Geophys. Res., 89(A5), 2891–2906.

Inan, U. S., M. Golkowski, M. K. Casey, R. C. Moore, W. Peter, P. Kulkarni, P. Kossey, E. Kennedy, S. Meth, and P. Smit (2007), Subionospheric VLF observations of transmitter-induced precipitation of inner radiation belt electrons, *Geophys. Res. Lett.*, 34, L02106, doi:10.1029/2006GL028494.

Jasna, D. U., U. S. Inan, and T. F. Bell (1992), Precipitation of suprathermal (100 eV) electrons by oblique whistler waves, Geophys. Res, Lett., 19(16), 1639-1642.

Johnson, M. P., U. S. Inan, S. J. Lev-Tov, and T. F. Bell (1999), Scattering pattern of lightning-induced ionospheric disturbances associated with early/fast VLF events, Geophys. Res, Lett., 26(15), 2363–2366.

Kennel, C. F., and H. E. Petschek (1966), Limit on stably trapped particle fluxes, J. Geophys. Res., 71(1), 1 – 28.

Lauben, D. S., U. S. Inan, and T. F. Bell (1999), Poleward-displaced electron precipitation from lightning-generated oblique whistlers, Geophys. Res. Lett., 26(16), 2633–2636.

Meredith, N.P., R. B. Horne, S. A. Glauert, R. M. Thorne, D. Summers, J. M. Albert, and R.R. Anderson (2006), Energetic outer zone electron loss timescales during low geomagnetic activity, J. Geophys. Res., 111, A05212, doi:10.1029/2005JA011516.

Meredith, N. P., R. B. Horne, S. Glauert, and R. R. Anderson (2007), Slot region electron loss timescales due to plasmaspheric hiss and lightning generated whistlers, J. Geophys. Res., 112, A08214, doi:10.1029/2007JA012413.

Molchanov, O., A. Rozhnoi, M. Solovieva, O. Akentieva, J. J. Berthelier, M. Parrot, F. Lefeuvre, P. F. Biagi, L. Castellana, and M. Hayakawa (2006), Global diagnostics of the ionospheric perturbations related to the seismic activity using the VLF radio signals collected on the DEMETER satellite, Nat. Hazards Earth Syst. Sci., 6, 745–753.

Peter, W. B., and U. S. Inan (2004), On the occurrence and spatial extent of electron precipitation induced by oblique nonducted whistler waves, J. Geophys. Res., 109, A12215, doi:10.1029/2004JA010412.

Rodger, C. J., M. A. Clilverd, and R. J. McCormick (2003), Significance of lightning generated whistlers to inner radiation belt electron lifetimes, J. Geophys. Res., 108(12), 1462, doi:10.1029/2003JA009906.

Rodger, C. J., M. A. Clilverd, Th. Ulich, P. T. Verronen, E. Turunen, and N. R. Thomson (2006), The atmospheric implications of radiation belt remediation, Ann. Geophys., 24, 2025–2041.

Saxton, J. M., and A. J. Smith (1989), Quiet time plasmaspheric electric fields and plasmasphere-ionosphere coupling fluxes at L = 2.5, Planet. Space Sci., 37, 283-293.

Smith, A. J., M. B. Grieve, M. A. Clilverd, and C. J. Rodger (2001), A quantitative estimate of the ducted whistler power within the outer plasmasphere, J. Atmos. Sol. Terr. Phys., 63, 61-74.

Strangeways, H. J. (1981), Trapping Of Whistler-Mode Waves In Ducts With Tapered Ends, J. Atmos. Terr. Phys., 43, 1071-1079.

Thomson, N. R. (1987a), Experimental observations of very low latitude man-made whistler-mode signals, J. Atmos. Terr. Phys., 49, 309-319.

Thomson, N. R. (1987b), Ray tracing the paths of very low latitude whistler-mode signals, J. Atmos. Terr. Phys., 49, 321-338.

Thorne, R. M., and R. B. Horne (1996), Whistler absorption and electron heating near the plasmapause, J. Geophys. Res., 101(A3), 4917-4928.

Van Allen, J. A. (1997), Energetic particles in the Earth's external magnetic field, in: Discovery of the Magnetosphere, edited by: Gillmor, C. S. and Spreiter, J. R., History of Geophysics, 7, AGU, Washington, D.C., 235–251.

Van Allen, J. A., G. H. Ludwig, E. C. Ray, and C. E. McIlwain (1958), Observation of high intensity radiation by satellites 1958 Alpha and Gamma, Jet Propulsion, 28, 588–592.

Jean-Jacques Berthelier, Centre d'Etudes des Environnements Terrestre et Planétaires, 4 Avenue de Neptune, Saint Maur des Fosses, France. (email: jean-jacques.berthelier@cetp.ipsl.fr).

M. A. Clilverd, and N. P. Meredith, Physical Sciences Division, British Antarctic Survey, High Cross, Madingley Road, Cambridge CB3 0ET, England, U.K. (e-mail: M.Clilverd@bas.ac.uk, nmer@bas.ac.uk).

R. J. Gamble, C. J. Rodger, and N. R. Thomson, Department of Physics, University of Otago, P.O. Box 56, Dunedin, New Zealand. (email: rgamble@physics.otago.ac.nz, crodger@physics.otago.ac.nz, thomson@physics.otago.ac.nz).

M. Parrot, Laboratoire de Physique et Chimie de l'Environnement, 3A Avenue de la Recherche Scientifique, 45071 Orleans Cedex 2, France (email: mparrot@cnrs-orleans.fr).

Table 1. Details of the transmitters used in this study, including the observed L-shell range of the peak wave power from each transmitter, and the likely electron precipitation energies (in keV) expected from each transmitter assuming parallel (0º wave normal angle) cyclotron resonance interactions at the field line geomagnetic equator. The energies of electrons precipitated by nonducted waves is likely to be higher than for ducted waves, and thus the energies are given in brackets to emphasize the uncertainty in this figure.

Transmitter call-sign, and Frequency (kHz)	**L-shell of transmitter**	**L-shell range of conjugate peak wave power**	**Range of resonant precipitation energies**
NPM, 21.4	**1.17**	**1.2-1.5**	**Nonducted (>500 keV)**
NWC, 19.8	**1.44**	**1.4-2.2**	**757 keV - 29 keV**
HWU, 18.3	**1.83**	**1.5-2.7**	**520 keV - 5 keV**
NSS, 21.4	**2.43**	**1.7-2.7**	**189 keV - 3 keV**
NAA, 24.0	**2.93**	**1.8-2.6**	**105 keV – 3 keV**

Figure Captions

Figure 1. (Left) The nighttime wave intensities of the NWC transmitter in Australia, in 2005, from DEMETER wave data covering the frequency range of 19.8 ± 0.01 kHz. (Right) CRRES wave data for 22.5 ± 0.45 kHz showing the nighttime wave intensities of the NWC transmitter in Australia in 1991.

Figure 2. A map of the locations of the regions of large intensity signals from the NWC transmitter in Australia. The circles represent signal intensities $>3 \times 10^2$ $\mu V^2 m^{-2} Hz^{-1}$ for DEMETER and $>10^1$ $\mu V^2 m^{-2} Hz^{-1}$ for CRRES. Observations made by DEMETER at 700 km above the transmitter (solid line), by CRRES at the equatorial plane of the magnetic field line (squares), and by DEMETER at 700 km altitude in the conjugate region (solid line) are shown, using the results from Figure 1. Contours for L=1.5, 2.0, 2.5, and the electron half-gyro frequency cutoff for 19.8 kHz ducted waves are also plotted.

Figure 3. (Left) The intensity of the HWU transmitter in France, in 2005, from DEMETER wave data covering the frequency range of 18.3 ± 0.01 kHz. (Right) CRRES wave data for 18.5 ± 0.45 kHz showing the intensity of the HWU transmitter in France in 1991.

Figure 4. A map of the locations of the regions of large intensity signals from the HWU transmitter in France. The circles represent signal intensities $>10^3$ $\mu V^2 m^{-2} Hz^{-1}$. Observations made from 700 km by DEMETER near the transmitter (solid line), by CRRES at the equatorial plane of the magnetic field line (squares), and by DEMETER at 700 km altitude in the conjugate region (solid line) are shown, using the results from Figure 3. Contours for L=1.5, 2.0, 2.5, and the electron half-gyro frequency cutoff for 18.3 kHz ducted waves are also plotted.

Figure 5. (Left) The intensity of the NAA transmitter in Maine, USA, in 2005, from DEMETER wave data covering the frequency range of 16.0 ± 0.01 kHz after Nyquist folding from 24.0 kHz about 20.0 kHz. (Right) CRRES wave data for 23.8 ± 0.45 kHz showing the intensity of the NAA transmitter in Maine, USA, in 1991.

Figure 6. A map of the locations of the regions of large intensity signals from the NAA transmitter in Maine, USA. The circles represent signal intensities >10^0 $\mu V^2 m^{-2} Hz^{-1}$ after attenuation from aliasing/Nyquist folding. Observations made by DEMETER from 700 km near the transmitter (solid line), by CRRES at the equatorial plane of the magnetic field line (squares), and by DEMETER at 700 km altitude in the conjugate region (dotted line) are shown, using the results shown in Figure 5. Contours for L=1.5, 2.0, 2.5, and the electron half-gyro and gyro frequency cutoff for 24.0 kHz ducted waves are also plotted.

Figure 7. A map of the location of the region of large intensity signals from the NSS transmitter in Washington, USA. The circle represents signal intensities >10^{-5} $mV^2 m^{-2} Hz^{-1}$. Only observations made at the equatorial plane of the magnetic field line (dashed line) are shown as NSS stopped operating before DEMETER became operational.

Figure 8. A map of the locations of the regions of large intensity signals from the 21.4 kHz NPM transmitter in Hawaii, USA. The circles represent signal intensities >3 x 10^2 $\mu V^2 m^{-2} Hz^{-1}$ after attenuation from aliasing/Nyquist folding. Observations made by DEMETER from 700 km altitude near the transmitter (solid line), and by DEMETER at 700 km altitude in the conjugate region are shown. The NPM signal (at 23.4 kHz in 1990/91) was not detectable in the CRRES data. Contours for L=1.5, and 2.0 are also plotted.

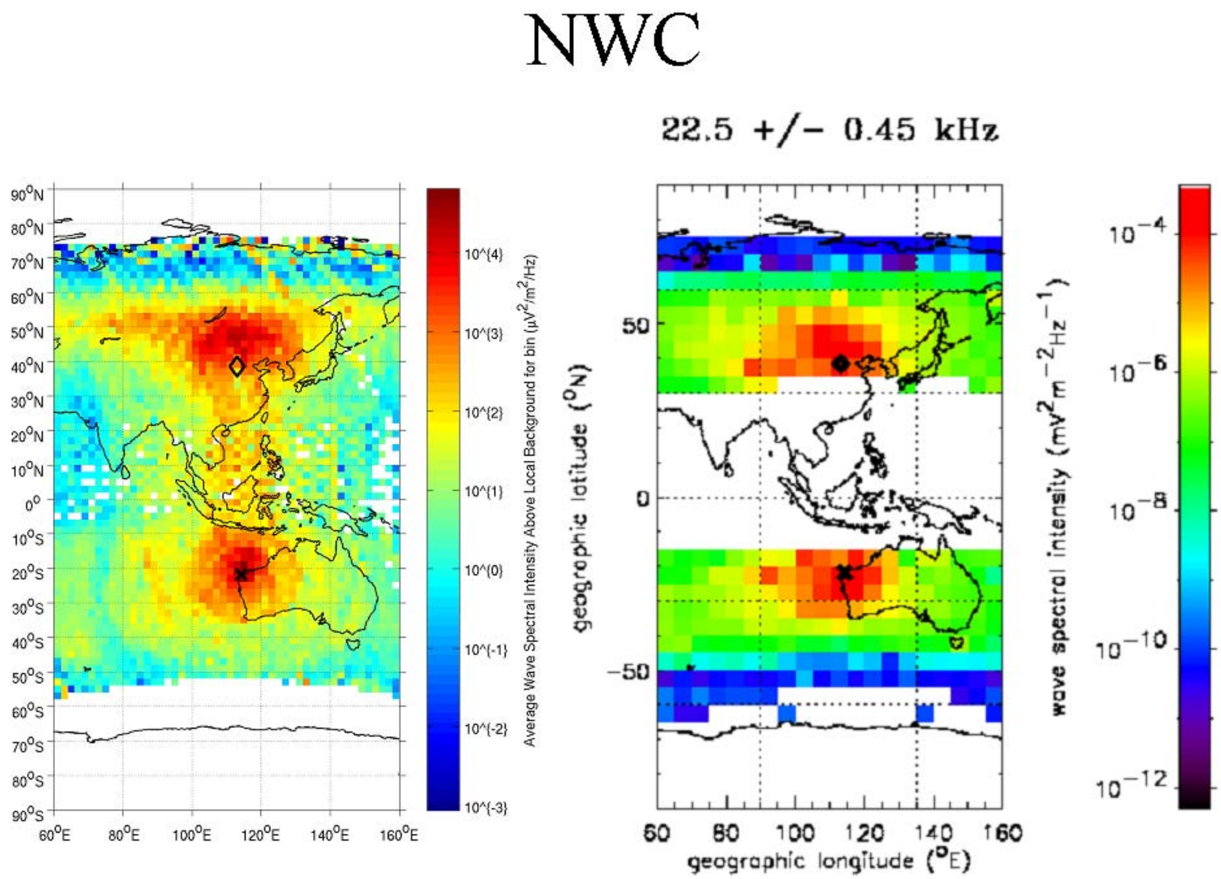

Figure 1. (Left) The nighttime wave intensities of the NWC transmitter in Australia, in 2005, from DEMETER wave data covering the frequency range of 19.8 ± 0.01 kHz. (Right) CRRES wave data for 22.5 ± 0.45 kHz showing the nighttime wave intensities of the NWC transmitter in Australia in 1991.

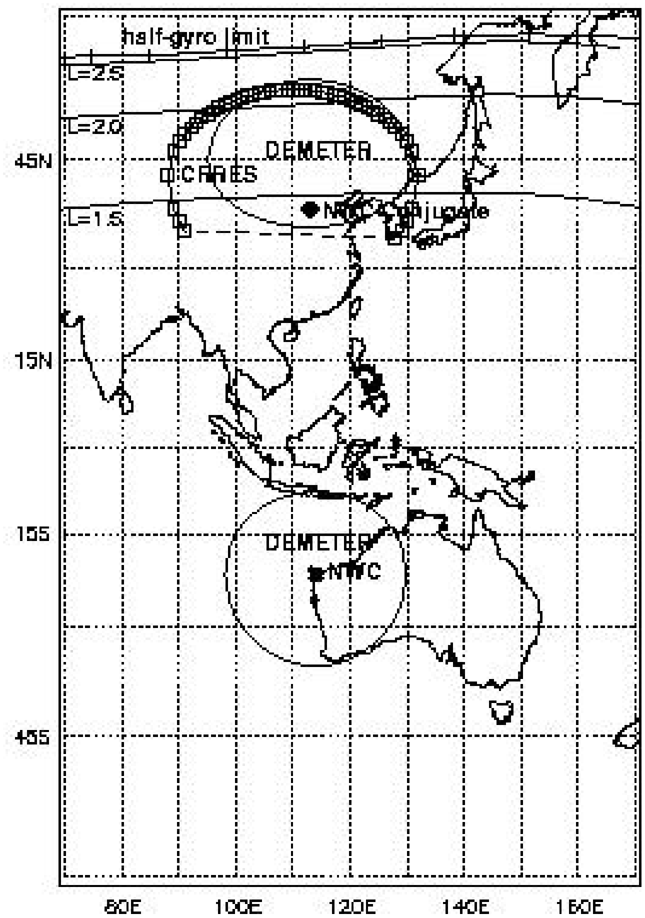

Figure 2. A map of the locations of the regions of large intensity signals from the NWC transmitter in Australia. The circles represent signal intensities >3 x 10^2 $\mu V^2 m^{-2} Hz^{-1}$ for DEMETER and >10^1 $\mu V^2 m^{-2} Hz^{-1}$ for CRRES. Observations made by DEMETER at 700 km above the transmitter (solid line), by CRRES at the equatorial plane of the magnetic field line (squares), and by DEMETER at 700 km altitude in the conjugate region (solid line) are shown, using the results from Figure 1. Contours for L=1.5, 2.0, 2.5, and the electron half-gyro frequency cutoff for 19.8 kHz ducted waves are also plotted.

HWU

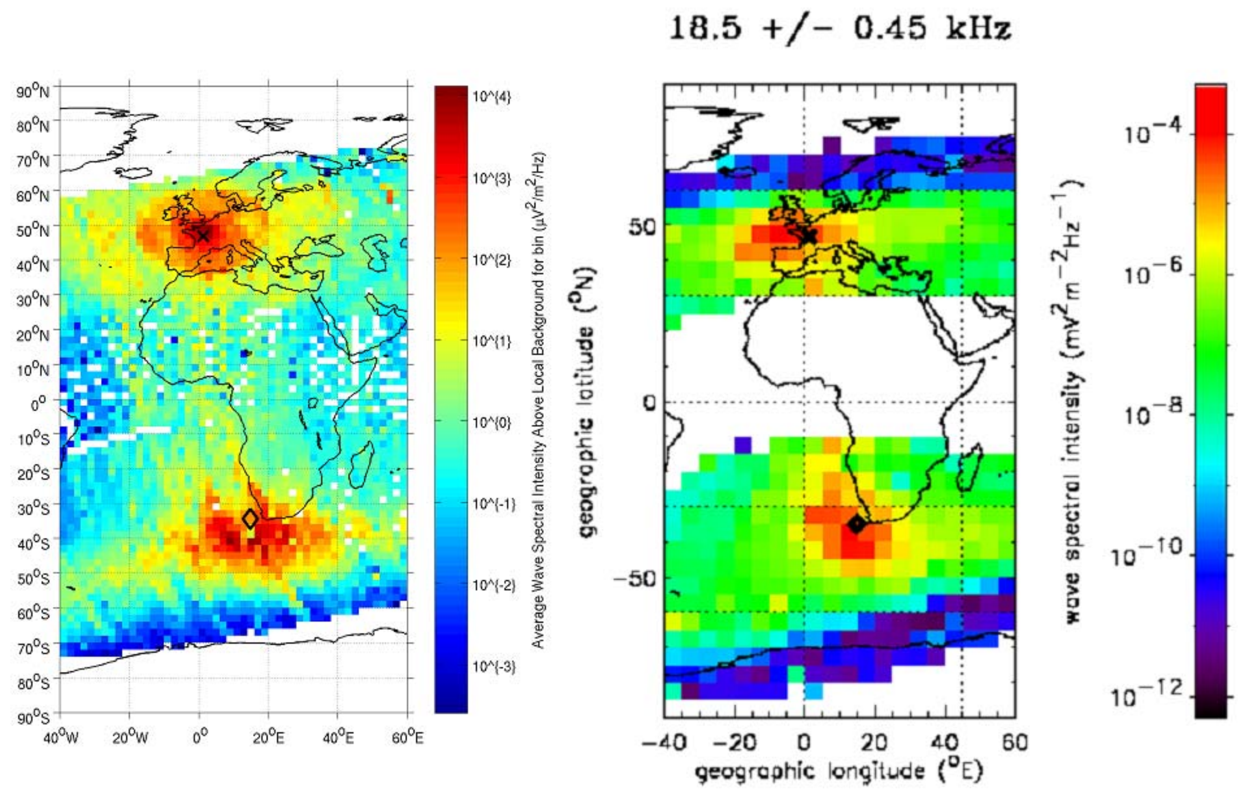

Figure 3. (Left) The intensity of the HWU transmitter in France, in 2005, from DEMETER wave data covering the frequency range of 18.3 ± 0.01 kHz. (Right) CRRES wave data for 18.5 ± 0.45 kHz showing the intensity of the HWU transmitter in France in 1991.

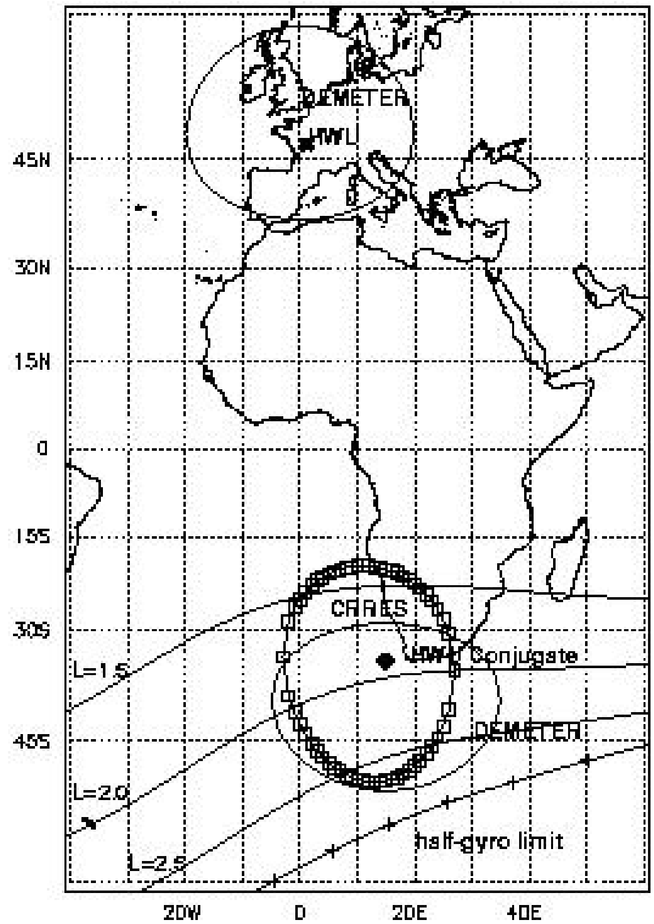

Figure 4. A map of the locations of the regions of large intensity signals from the HWU transmitter in France. The circles represent signal intensities $>10^3\ \mu V^2 m^{-2} Hz^{-1}$. Observations made from 700 km by DEMETER near the transmitter (solid line), by CRRES at the equatorial plane of the magnetic field line (squares), and by DEMETER at 700 km altitude in the conjugate region (solid line) are shown, using the results from Figure 3. Contours for L=1.5, 2.0, 2.5, and the electron half-gyro frequency cutoff for 18.3 kHz ducted waves are also plotted.

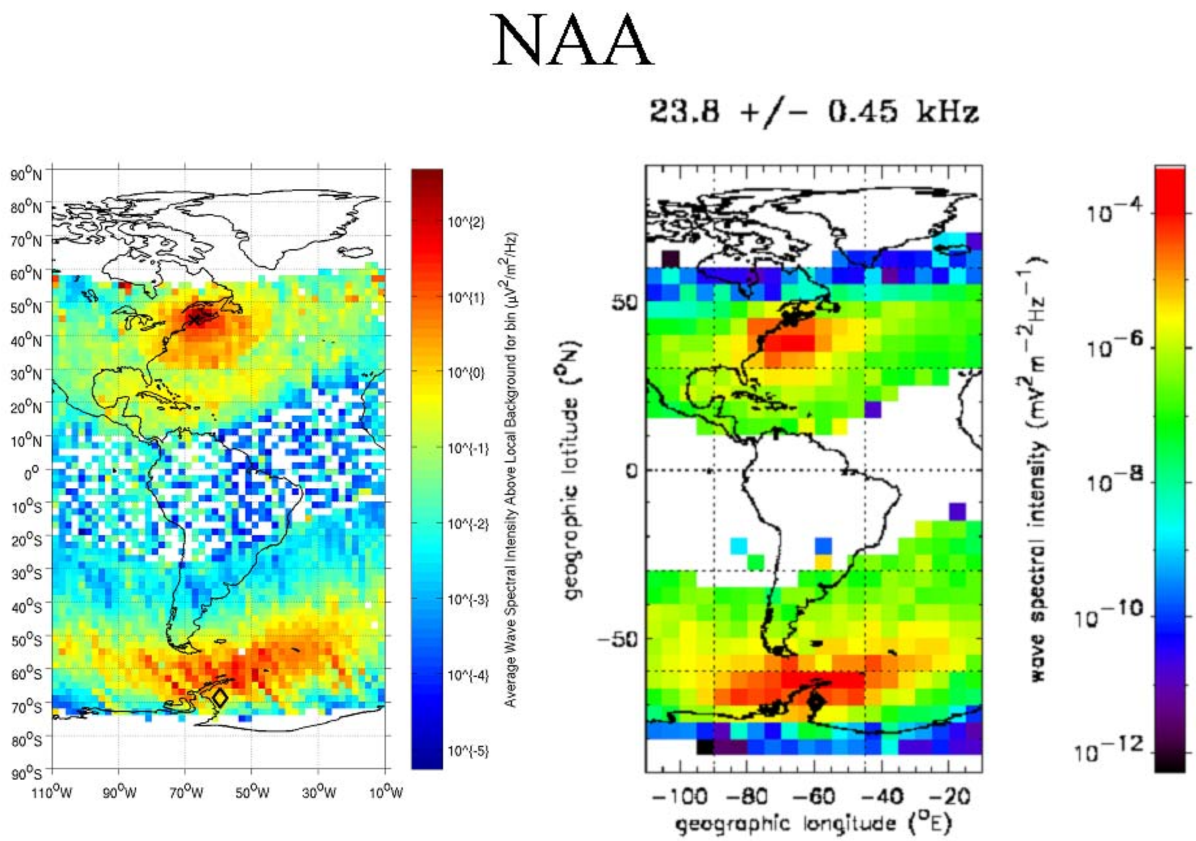

Figure 5. (Left) The intensity of the NAA transmitter in Maine, USA, in 2005, from DEMETER wave data covering the frequency range of 16.0 ± 0.01 kHz after Nyquist folding from 24.0 kHz about 20.0 kHz. (Right) CRRES wave data for 23.8 ± 0.45 kHz showing the intensity of the NAA transmitter in Maine, USA, in 1991.

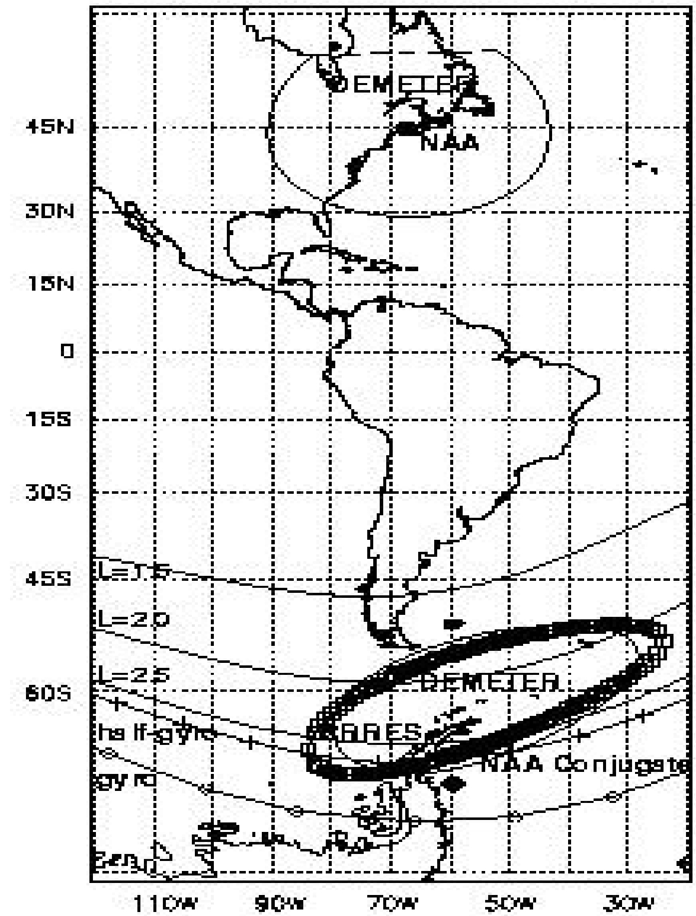

Figure 6. A map of the locations of the regions of large intensity signals from the NAA transmitter in Maine, USA. The circles represent signal intensities $>10^0\ \mu V^2 m^{-2} Hz^{-1}$ after attenuation from aliasing/Nyquist folding. Observations made by DEMETER from 700 km near the transmitter (solid line), by CRRES at the equatorial plane of the magnetic field line (squares), and by DEMETER at 700 km altitude in the conjugate region (dotted line) are shown, using the results shown in Figure 5. Contours for L=1.5, 2.0, 2.5, and the electron half-gyro and gyro frequency cutoff for 24.0 kHz ducted waves are also plotted.

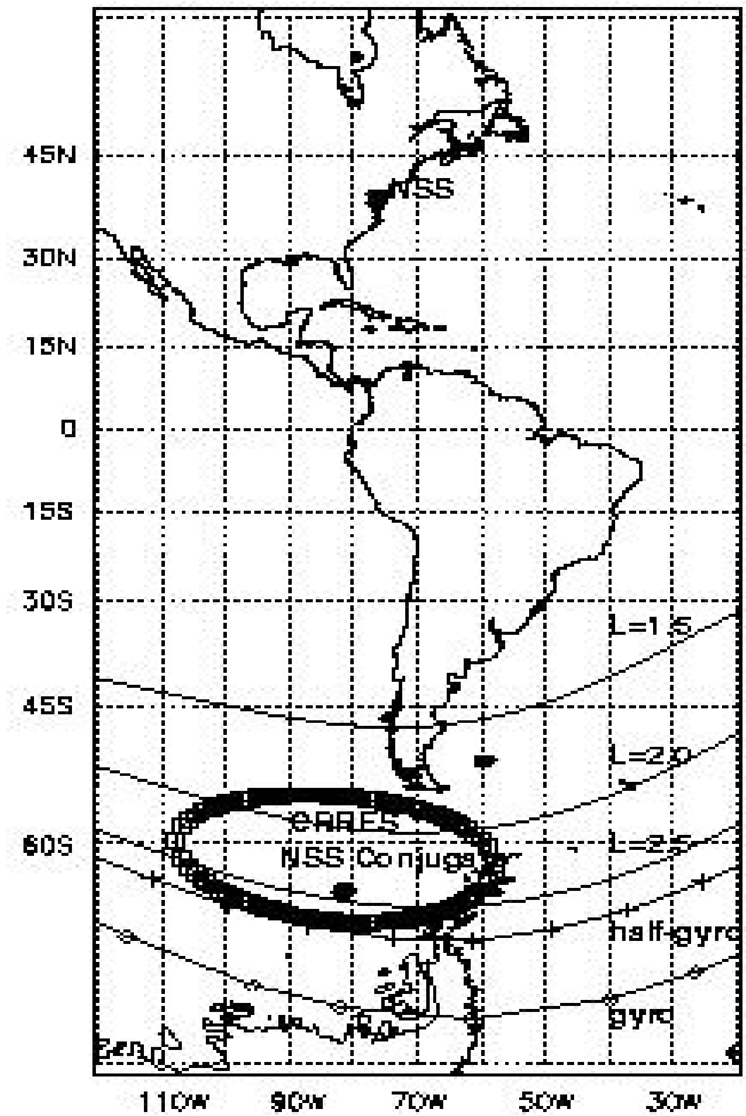

Figure 7. A map of the location of the region of large intensity signals from the NSS transmitter in Washington, USA. The circle represents signal intensities $>10^{-5}$ $mV^2m^{-2}Hz^{-1}$. Only observations made at the equatorial plane of the magnetic field line (dashed line) are shown as NSS stopped operating before DEMETER became operational.

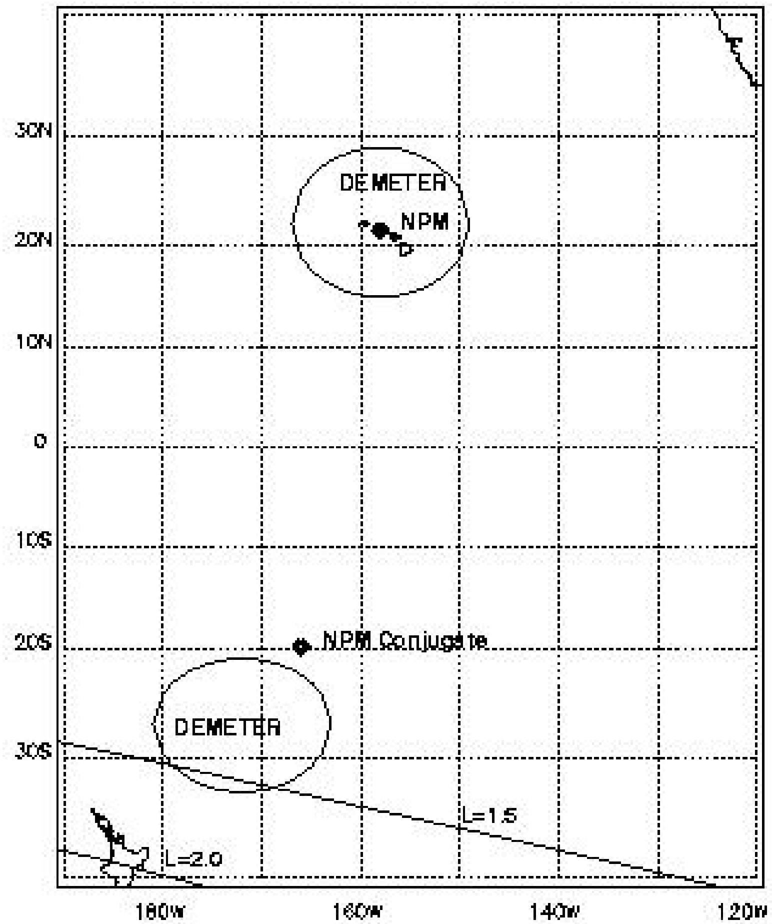

Figure 8. A map of the locations of the regions of large intensity signals from the 21.4 kHz NPM transmitter in Hawaii, USA. The circles represent signal intensities $>3 \times 10^2\ \mu V^2 m^{-2} Hz^{-1}$ after attenuation from aliasing/Nyquist folding. Observations made by DEMETER from 700 km altitude near the transmitter (solid line), and by DEMETER at 700 km altitude in the conjugate region are shown. The NPM signal (at 23.4 kHz in 1990/91) was not detectable in the CRRES data. Contours for L=1.5, and 2.0 are also plotted.